

Vortical structures in the wake of a rim-driven thruster operating at maximum efficiency

Maarten Vanierschot^{1,2*}, Wu Ouyang³ and Bao Liu³

¹ KU Leuven, Department of Mechanical Engineering, Leuven 3001, Belgium

² North-West University, Material Science, Innovation and Modelling (MaSIM) Research Focus Area, Mmabatho 2745, South Africa

³ School of Transportation and Logistics Engineering, Wuhan University of Technology, Wuhan 430063, People's Republic of China

*mailto: maarten.vanierschot@kuleuven.be

Abstract

The rim-driven thruster (RDT) has drawn much attention worldwide and experienced rapid development. Instead of being shaft-driven as in a traditional propulsion system, RDTs have a much more compact design by integration of the driving motor with the propeller. The structure of an RDT resembles a ducted propeller, yet without a tip clearance as the propeller is directly connected to the rim. Despite being an emerging technology, the flow structures present in the wake of RDTs are still largely unknown. However, the structure and dynamics of the RDT wake are crucial in performance prediction and estimation of noise production. Therefore, this paper studies the vortical structures found in the wake of an RDT operating at maximum efficiency. Delayed detached eddy simulations are performed and the wake flow is analyzed using both visualization of the instantaneous vortical structures and large scale structure extraction by proper orthogonal decomposition (POD). Three main structures have been identified. The first one is the central hub vortex, which is the strongest one and it is aligned with the flow direction and precesses around the central axis of the RDT. Next to the hub vortex, small scale vortices are formed after the duct in the shear layer between the wake flow and the surrounding and these are convected downstream. The last structures are the trailing vortices shed by the propeller blades and these are dissipated quite fast downstream.

1 Introduction

Study of the vortical structures in the wake of marine propellers is very important since they contribute to a large extend to the noise production as their dynamical evolution is largely responsible for the oscillations and noise performance of the propeller (Baek et al., 2015). When water passes through the blades, interactions between the flow and propeller induce noise and vibrations, which are mainly related to the propeller geometry and loading (Viitanen et al., 2018). Coherent vortical structures are generated by the propeller blades and they are convected downstream in the wake. Moreover, vortices shed from different parts of the propeller often exhibit strong self- and mutual induction, causing instabilities and associated break-up (Gong et al., 2018).

In order to increase the thrust at lower speeds, propellers are often accompanied by a duct, i.e. the so-called ducted propeller (DP). However, the presence of a duct complicates the structure and interaction of the wake vortices. Tip leakage vortices are formed due to the tip clearance between the blade tip and the duct's interior surface. At the trailing edge of the duct, flow separation interacts with the propeller tip vortices, causing different wake evolution patterns compared to open propellers (Gong et al., 2018). A recent 'ducted propeller' technology is the rim-driven thruster (RDT), which integrates the propeller and motor (Yan et al., 2017). In contrast to a traditional DP, there is no tip clearance and therefore no tip leakage vortices are present. To avoid this tip clearance, a channel of small dimensions, i.e. the rim, is present which induces a gap flow. This gap flow has a significant influence on the overall performance of the thruster and results in a lower efficiency compared to a traditional DP (Liu and Vanierschot, 2021). Therefore, it is particularly important to design RDT geometries carefully for optimal performance.

As the wake structure has a significant impact on the noise production, experimental methods can be used to study its structure. However, they can be costly and time consuming or limited information can be extracted. Therefore, numerical simulations are a good alternative, as they can provide more detailed information on the flow field structure. These simulations include RANS turbulence models (Baek et al., 2015; Liu and Vanierschot, 2021), delayed detached eddy simulations (Wang et al., 2021; Viitanen et al., 2018; Liu et al., 2024) or large eddy simulations (Zhu and Gao, 2019). In contrast to ducted propellers, numerical studies



on the details of the vortical structures in the wake of an RDT are much more scarce. Therefore, this work aims to study the wake characteristics of an RDT operating at maximum efficiency to fill this knowledge gap. To analyse the wake, both instantaneous vortical structures are presented, as well as a proper orthogonal decomposition (POD) to highlight the coherent structures which are precessing around the central axis of the RDT wake.

2 Materials and methods

2.1 Governing equations

The ensemble averaged or filtered governing equations for incompressible Newtonian turbulent fluid flows are given in tensor notation as:

$$\frac{\partial \bar{u}_i}{\partial x_i} = 0, \quad (1)$$

$$\frac{\partial \bar{u}_i}{\partial t} + \bar{u}_j \frac{\partial \bar{u}_i}{\partial x_j} = -\frac{1}{\rho} \frac{\partial \bar{p}}{\partial x_i} + \nu \frac{\partial^2 \bar{u}_i}{\partial x_j \partial x_j} - \frac{\partial \tau_{ij}}{\partial x_j}, \quad (2)$$

where ρ is the fluid density, \bar{u}_i ($i, j = 1, 2, 3$) is the ensemble averaged or filtered velocity component, t is the flow time, p is the pressure, ν is the kinematic viscosity, and τ_{ij} is the residual stress tensor. In this study, turbulence is modeled using the Delayed Detached Eddy Simulation (DDES) approach as this model gives very good results for RDT flows (Liu et al., 2024). For the RANS component of the DDES, an SST $k - \omega$ model (Menter, 1994) and for the LES component, the dynamic Smagorinsky-Lilly model (Lilly, 1992) are used as turbulence closures. ANSYS Fluent is used as numerical solver. Second-order central differencing schemes are used for the discretization of the momentum equation, while a second order upwind scheme is used for the turbulence equations. The SIMPLEC algorithm is adopted for the pressure-velocity coupling. For the temporal discretisation, a second order scheme is used and the timestep, $t = 1 \times 10^{-5}$ s, is chosen to have a maximum Courant number in the order of 1 and an average Courant number of 0.08 in the rotating domain.

2.2 Numerical domain, grid generation and boundary conditions

The geometrical models used in this study are presented in figure 1. The computational domain is a cylinder with a length of $10D$ and a radius of $4D$, where $D = 0.1$ m is the diameter of the propeller, as shown in figure 1(b). In the used cartesian coordinate system, the axial direction corresponds to the z -axis. The velocity inlet is located $2D$ upstream of the propeller and the pressure outlet is situated $8D$ downstream. This setting was observed to avoid confinement effects while not influencing the evolution of the wake flow (Mahesh et al., 2015; Gong et al., 2018). Previous work has shown that the maximum efficiency of the RDT corresponds to an advance ratio of $J = 0.5$ (Liu and Vanierschot, 2021). This gives a mean value of the inlet velocity of 1 m/s. On this mean profile, random turbulent fluctuations are superimposed, resembling a 5% free stream turbulence

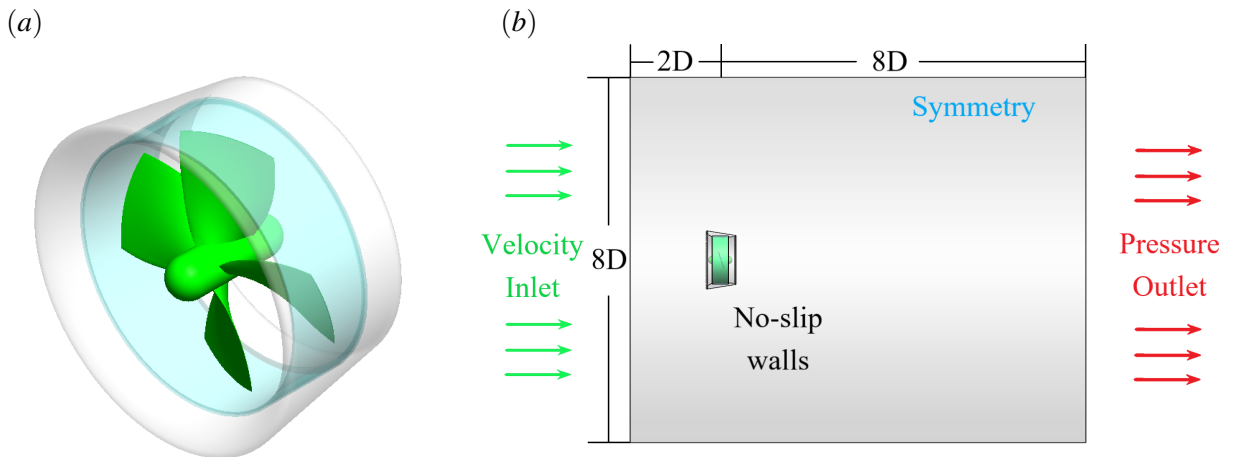


Figure 1. Schematic view of the numerical setup: (a) the RDT geometry (DP) and (b) the computational domain and boundary conditions.

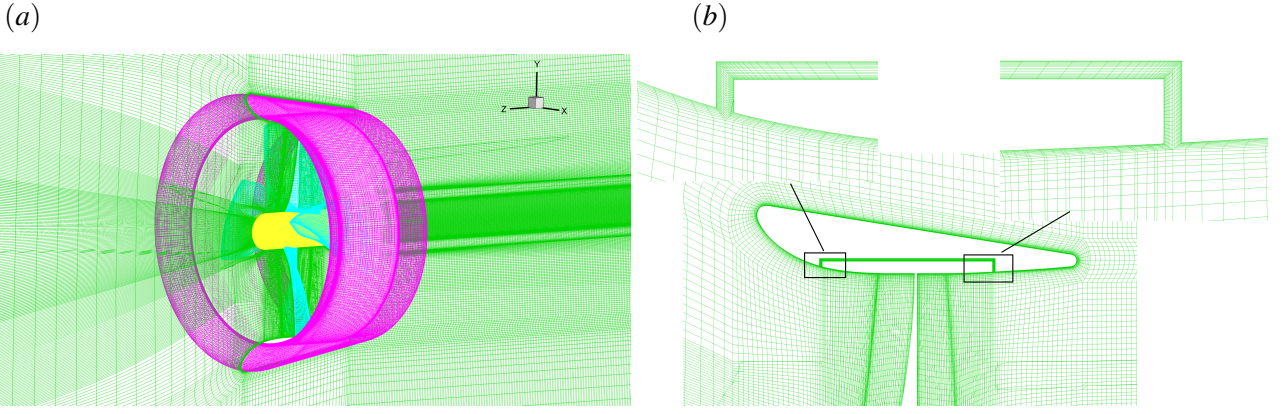


Figure 2. The mesh employed in the simulations: (a) general structure of the mesh, (b) detailed view of the region around the propeller, including the rim.

intensity. At the pressure outlet, Neumann boundary conditions are applied. The side surface of the domain is implemented as a slip wall boundary condition. The computational domain consists of a static zone and a rotating zone containing the propeller, rim and hub. To simulate the rotational movement of the propeller, the sliding mesh (SM) approach is employed. The rotational rate of this rotating zone is $n = 20$ revolutions per second. A fully structured mesh of about 24.5 million cells (figure 2) ensures that in the wake region at least 85% of the turbulent kinetic energy is resolved, which means the LES component of the DDES is well resolved. More information on the mesh can be found in our previous work (Liu et al., 2024).

2.3 Coherent structure analysis

To analyse the coherent structures in the flow field, proper orthogonal decomposition (POD) is applied. The flow field $u(x, t) = (u, v, w)$ is decomposed into a time averaged ($\langle u(x, t) \rangle$) and a fluctuation ($u^\dagger(x, t)$) part as

$$u(x, t) = \langle u(x, t) \rangle + u^\dagger(x, t). \quad (3)$$

The fluctuating part is written as a collection of spatial modes:

$$u(x, t) = \langle u(x, t) \rangle + u^\dagger(x, t) = \langle u(x, t) \rangle + \sum_{i=1}^N a_i(t) \Phi_i(x), \quad (4)$$

where $\Phi_i(x)$ represents a spatial POD mode and $a_i(t)$ is the corresponding temporal coefficient. The influence of different modes on the flow can be analysed by reconstruction of the flow field in eq. 3 with only the specific modes i of interest involved.

3 Results and Discussion

As pressure fluctuations and vortical structures are largely responsible for the sound generation and propagation, the analysis of the flow field will mainly focus on those. To indicate regions of high fluctuations, the turbulent kinetic energy and the root-mean-square of the pressure coefficient are shown in figure 3. The pressure coefficient is defined as

$$C_p = \frac{p - p_\infty}{0.5\rho(nD)^2}, \quad (5)$$

where p is the local static pressure, p_∞ the free-stream pressure and D the propeller diameter. The resolved turbulent kinetic energy in Figure 3(a) shows large values behind the hub. These fluctuations are caused by the hub vortex, which is the most dominant flow structure in the wake, similar to other loading regimes (Liu et al., 2024). Compared to bollard conditions, i.e. zero sailing velocity of the ship, the hub vortex is even stronger. Another region of high fluctuations is the shear layer between the wake and surrounding flow behind

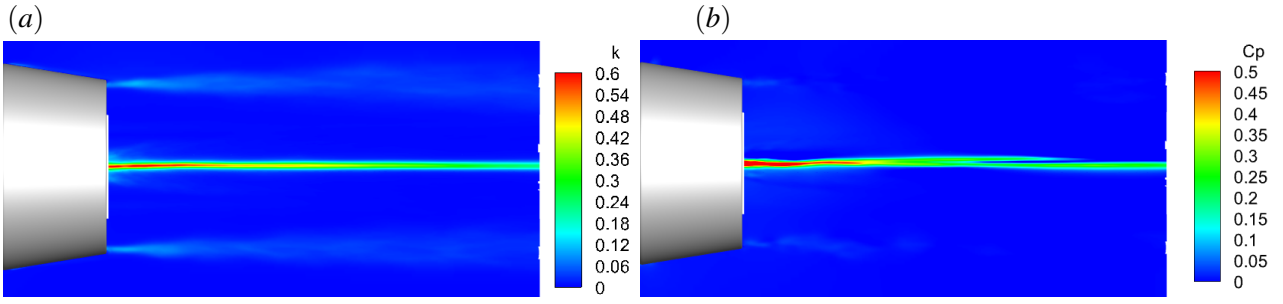


Figure 3. Regions in the flow field with high fluctuations: (a) mean turbulent kinetic energy and (b) root-mean-square of the pressure coefficient.

the duct. However, the turbulent kinetic energy in that region is much smaller compared to the hub vortex. In bollard conditions, this difference is less pronounced. The pressure fluctuations are shown in figure 3(b). It can be observed that the general profile is very similar to the one of the turbulent kinetic energy, with the major fluctuations concentrated in the hub region and lower values in the outer shear layer.

3.1 Instantaneous flow structures

The instantaneous vortical structures in the wake field of the RDT are identified using the Q -criterion (Jeong and Hussain, 1995). Q is defined based on the velocity gradient tensor $\nabla\bar{\mathbf{U}}$ as

$$Q = \frac{1}{2}(\|\boldsymbol{\Omega}\|^2 - \|\mathbf{S}\|^2), \quad (6)$$

where $\Omega_{ij} = \frac{1}{2}(\bar{U}_{i,j} - \bar{U}_{j,i})$ and $S = \frac{1}{2}(\bar{U}_{i,j} + \bar{U}_{j,i})$ are the vorticity and shear strain rate tensor respectively, which represent the symmetric and antisymmetric components of $\nabla\bar{\mathbf{U}}$. The vortical structures at an arbitrarily time instant are shown in figure 4 for $Q = 5000$ 1/s. The iso-surfaces are colored by the local axial (stream-wise) velocity. It can be clearly seen that the propeller wake flow is very complex, with numerous turbulent small-scale coherent structures distributed along the streamwise direction in an irregular manner. This highly turbulent nature of the wake has also been observed by Gaggero (2023), making it hard to identify a representative helical vortex system as found in conventional open propellers. Nevertheless, a distinct large scale vortical structure can be found behind the hub, called the hub vortex. This vortex is formed due to the bluff-body nature of the hub and the dynamics of this vortex is responsible for the high fluctuations in variables near the center of the RDT (figure 3). The hub vortex is very strong and is present in the flow field up to the outlet of the

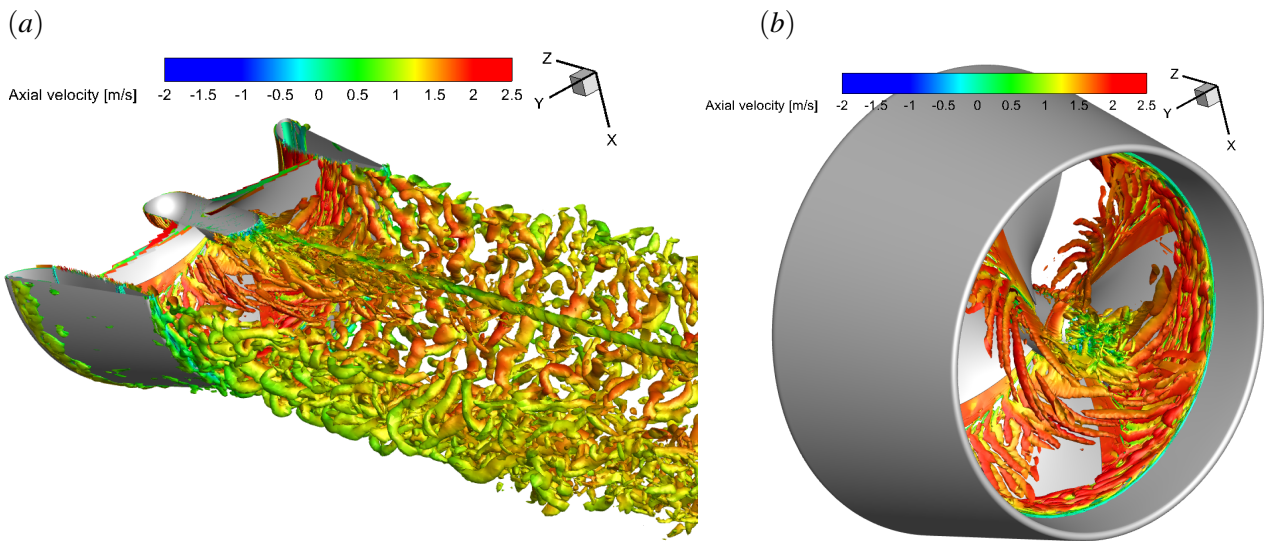


Figure 4. Instantaneous flow structures in the RDT wake, visualised using isosurfaces of $Q = 5000$ 1/s. The isosurfaces are colored according to axial velocity, (a) overview of the general wake where the upper half of the domain is blanked to increase visibility and (b) close up near the propeller blades, where everything downstream of the duct is blanked for readability.

numerical domain ($8D$ behind the propeller). Smaller vortical structures can also be found behind the duct in the shear layer between the propeller wake and surrounding flow. These vortices are convected downstream for several propeller diameters before they break up and are dissipated. A close zoom near the propeller blades in figure 4(b) shows that at the trailing edge of the blade, vortices are also shed. These trailing vortices however dissipate very fast and are only restricted to a very small region after the blades.

3.2 POD results

As can be seen from figure 4, the flow structures in the wake are very complex and large scale structures are masked by smaller turbulent ones. In order to be able to analyse these large scale structures, the flow field is decomposed using POD. In a classical POD analysis, the modes are ordered according to energy content. However, in this case we are looking for coherent rotating structures, which do not necessarily have the highest energy (Zhang and Vanierschot, 2021). Instead, it is better to look for mode pairs, i.e. two linked modes which have the same spectral content and a constant phase difference between the temporal coefficients. As such, reconstructing the flow field with a mode pair describes the precession of a coherent structure. A linked mode pair can be identified by looking at the harmonic correlation of the eigenvectors of the dynamic mode decomposition of the temporal coefficients. The higher the harmonic correlation, the better the modes describe a precession. More detailed information on the identification of the pairs can be found in the work of Sieber et al. (2016). A representative POD spatial mode with associated time coefficient is shown in figure 5. Only half of the domain is shown for clarity. The modes are visualized using iso-surfaces of static pressure. These iso-surfaces allow visualization of coherent structures behind the blades of the propeller, as well as the presence of vortex cores (Liu et al., 2024). From figure 5(a), three distinct regions containing coherent structures can be identified. The first region is located around the central axis and represents the hub vortex. The second region can be found near the blades, which represents fluctuations caused by the leading and trailing edges of the blades and the formation of the trailing vortices. The last region is located behind the duct and these structures represent the shear layer between wake and surrounding flow. The same regions were also identified in figure 4. The corresponding temporal coefficient is shown in figure 5(b). The time axis corresponds to one period of the propeller's rotation and hence this structure has a frequency of $4n$. In the following analysis, the POD modes are very similar to the ones in figure 5 and to avoid similar duplicate figures, the temporal coefficients will be discussed in terms of frequency and their graphical representation will not be shown anymore. Also, the spatial POD structures behind the duct will be blanked in the remainder of the paper to enhance readability of the figures.

The spatial structure of the mode pair with the highest harmonic correlation is shown in figure 6. This pair will further be referred to as pair I. The structure of both modes in the pair is very similar to the representative mode in figure 5. This mode pair describes both the central hub vortex and the shear layer between wake and surroundings, as well as pressure fluctuations at the blade's leading and trailing edges. This shows the

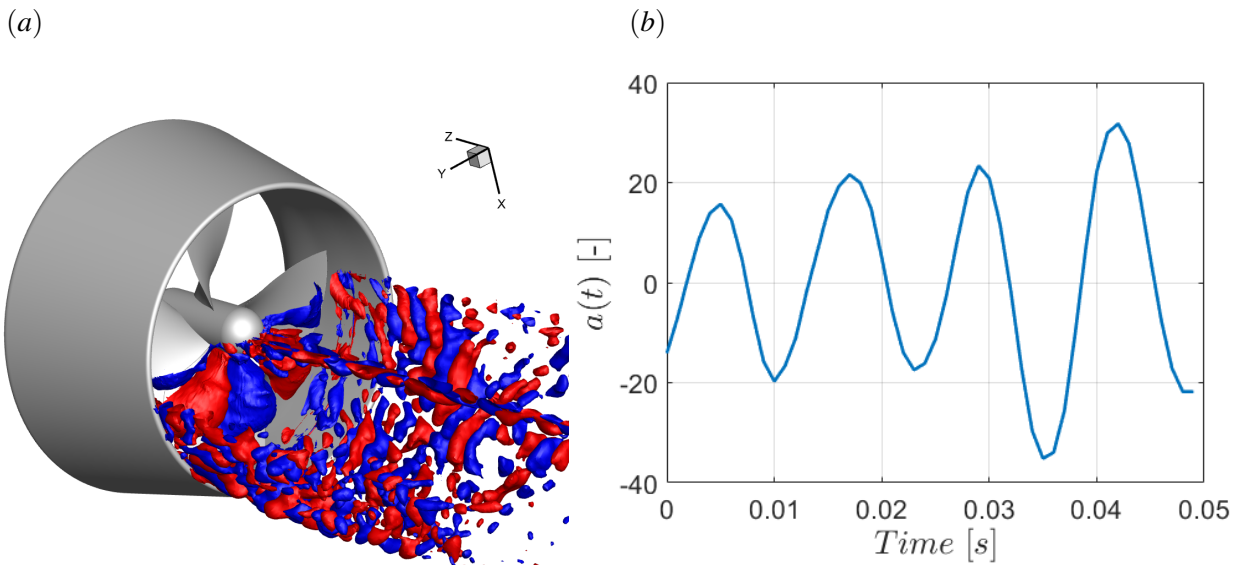


Figure 5. Representative mode (mode 6 in the POD decomposition): (a) spatial component visualised by iso-surfaces of pressure. The red isosurfaces are values of $P = -1$ Pa and the blue isosurfaces of $P = 1$ Pa. Half of the domain is blanked for increased visibility, (b) associated temporal coefficient.

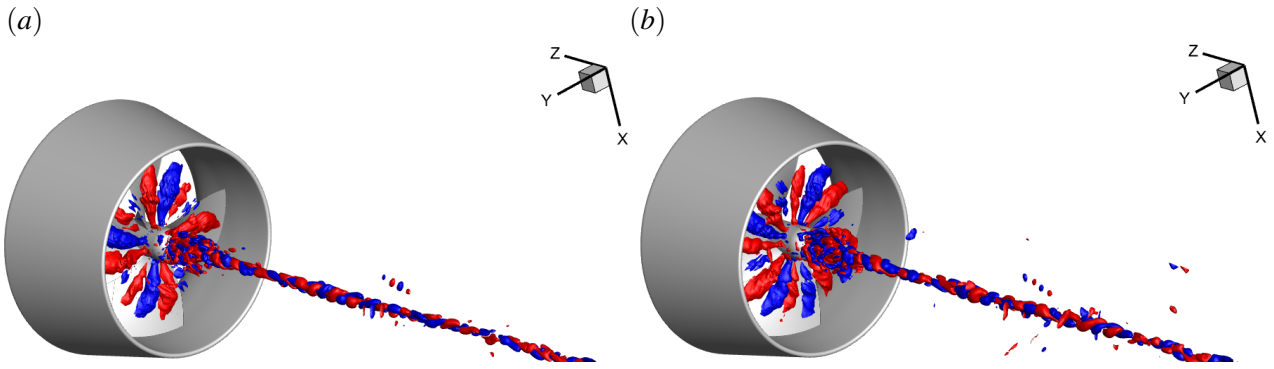


Figure 6. Mode pair with the highest harmonic correlation (pair I). The red isosurfaces are values of $P = -1$ Pa and the blue isosurfaces of $P = 1$ Pa. (a) First mode of the pair (3.2% energy content), (b) Second mode of the pair (3.1% energy content).

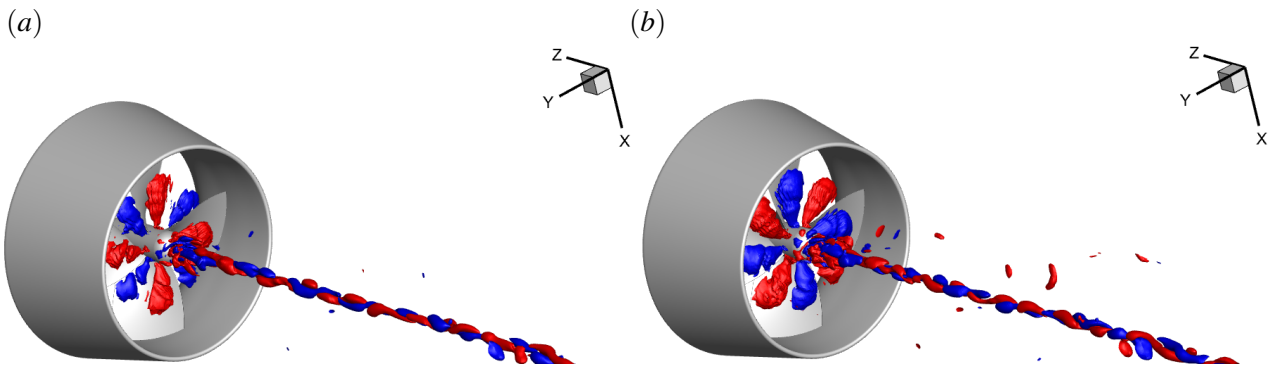


Figure 7. Mode pair with the second highest harmonic correlation (pair II). The red isosurfaces are values of $P = -1$ Pa and the blue isosurfaces of $P = 1$ Pa. (a) First mode of the pair (12% energy content), (b) Second mode of the pair (10% energy content).

strong coherence between the three distinct regions in the flow field as they can be captured within the same POD modes. Moreover, since they have the same temporal coefficient, their temporal dynamics is the same. A spectral analysis of the time coefficients associated with this mode pair shows a dominating frequency of 80Hz, equal to $4n$. The energy content of the mode pair is not very high, with only about 3% for each mode of the pair.

The mode pair with the second highest harmonic correlation (pair II) is shown in figure 7. Similar to pair I, it represents the hub vortex, the shear layer of the wake and the leading and trailing edges' fluctuations. The associated temporal coefficients show a distinct peak at 2 times the rotational speed of the propeller ($2n$). The energy content is also higher than pair I, in the order of 11%. The structure of pair II is very similar to pair I and analysis of the temporal coefficients by mean of Lissajous figures (not shown here) shows that pair I is the second harmonic of pair II. This harmonic relation is also present spatially: near the blades, pair II has an

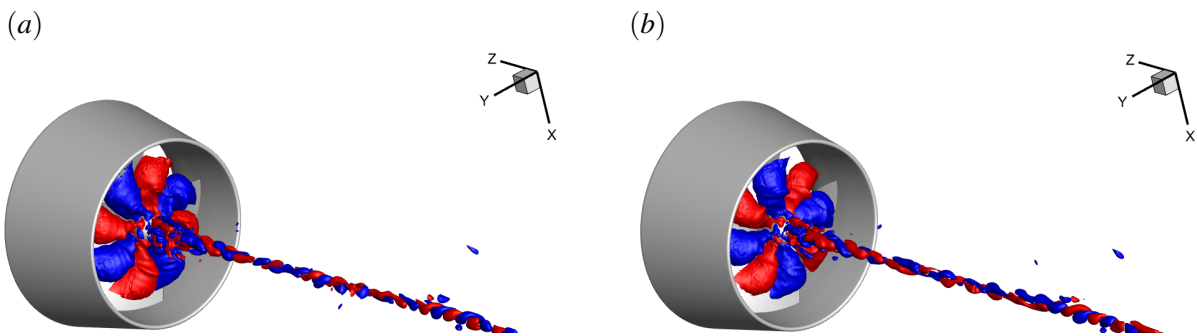


Figure 8. Mode pair with the third highest harmonic correlation (pair III). The red isosurfaces are values of $P = -1$ Pa and the blue isosurfaces of $P = 1$ Pa. (a) First mode of the pair (8% energy content), (b) Second mode of the pair (7% energy content).

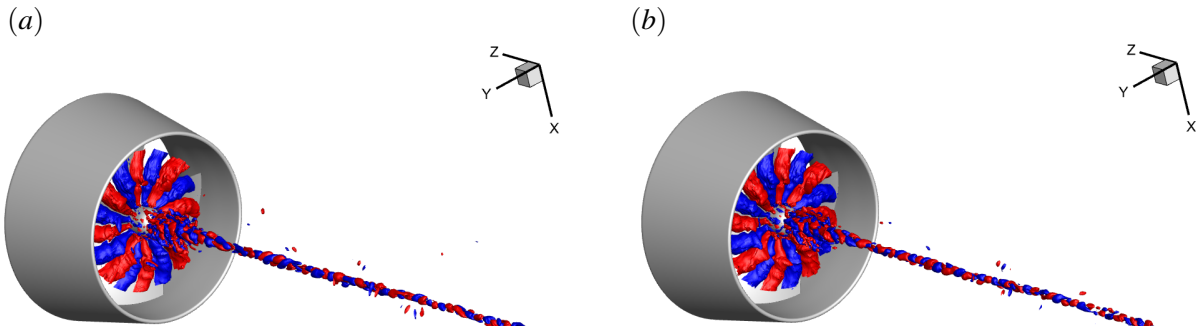


Figure 9. Mode pair with the fourth highest harmonic correlation (pair IV). The red isosurfaces are values of $P = -1$ Pa and the blue isosurfaces of $P = 1$ Pa. (a) First mode of the pair (2.3% energy content), (b) Second mode of the pair (2.2% energy content).

azimuthal wavenumber of $m = 4$, while the azimuthal wavenumber of pair I is $m = 8$.

The mode pair with the third highest harmonic correlation (pair III) is shown in figure 8. The structure is again very similar to the previous modes. The temporal coefficients show a frequency spectrum with a peak at $4n$. Despite that the azimuthal wavenumber is also $m = 4$, no relation could be found in the temporal coefficients between pair III and pairs I and II. In figure 9, the mode pair with the fourth highest harmonic correlation is shown (pair IV). Since the azimuthal wavenumber is $m = 8$ and the temporal coefficient shows a peak at $4n$, pair IV is the second harmonic of pair III, which is also confirmed by the Lissajous figures of the temporal coefficients. As was the case with pair III, no relation could be found with pairs I and II.

4 Conclusions

This paper analyses the wake structures of a rim-driven thruster operating a maximum efficiency. The wake is analysed by both looking at the instantaneous vortical structures, as well as the POD modes with the highest harmonic correlation, representing precessing structures. Three distinct regions of coherence can be identified: the first region is near the central axis, representing the hub vortex. This is the strongest structure in the flow field. The second region is behind the blades, where the leading and trailing edges induce fluctuations in flow quantities. The last identified region is the shear layer between wake and surroundings. The POD analysis shows that the structure of the modes with the highest correlation is very similar, showing that the coherent structures in the wake of the RDT are highly correlated as they are present in each mode. Moreover they have the same temporal dynamics, giving by their common temporal coefficients. This dynamics can be described by two mode pairs with frequencies of 2 and 4 times the rotational rate of the propeller and their associated second harmonics.

Acknowledgments

This project was financially supported by the National Key R&D Program of China (No.2022YFB4300802) and the Fundamental Research Funds for the Central Universities (WUT:2023IVA084). The computational resources and services used in this work were provided by the VSC (Flemish Supercomputer Center), funded by the Research Foundation - Flanders (FWO) and the Flemish Government – department EWI.

References

- Baek, D., Yoon, H., Jung, J., Kim, K., Paik, B. 2015, Effects of the advance ratio on the evolution of a propeller wake, *Comput. Fluids*, **118**, 32–43.
- Gaggero, S., 2023, A study on the wake evolution of a set of rim-driven thrusters, *J. Mar. Sc. Eng.*, **11**, 1659.
- Gong, J., Guo, C., Zhao, D., Wu, T., Song, K. 2018, A comparative DES study of wake vortex evolution for ducted and non-ducted propellers, *Ocean Eng.*, **160**, 78–93.
- Jeong, J., Hussain, F., 1995, On the identification of a vortex, *J. Fluid Mech.*, **285**, 69–94.
- Lilly, D.K. 1992, A Proposed Modification of the Germano Subgrid-Scale Closure Model, *Phys. Fluids.*, **4**, 633–635.

- Liu, B., Vanierschot, M. 2021, Numerical study of the hydrodynamic characteristics comparison between a ducted propeller and a rim-driven thruster, *Appl. Sc.-Basel*, **11**, 4919.
- Liu, B., Yan, X., Ouyang, W., Vanierschot, M. 2024, Comparison study of the vortical structures in the wake of a rim-driven thruster and a ducted propeller in bollard conditions, *Ocean Eng.*, **306**, 118064.
- Mahesh, K., Kumar, P., Gnanaskandan, A., Nitzkorski, Z. 2015, LES applied to ship research, *J. Ship Res.*, **59**, 238–245.
- Menter, F. 1994, Two-equation eddy-viscosity turbulence models for engineering applications, *AIAA J.*, **32**, 1598–1605.
- Sieber M., Paschereit, C.O., Oberleithner, K. 2016, Spectral proper orthogonal decomposition, *J. Fluid Mech.*, **792**, 798–828.
- Viitanen, V., Hynninen, A., Sipilä, T., Siikonen, T. 2018, DDES of wetted and cavitating marine propeller for CHA underwater noise assessment, *J. Mar. Sc. Eng.*, **6**, 56.
- Wang, L., Wu, T., Gong, J., Yang, Y. 2021, Numerical analysis of the wake dynamics of a propeller, *Phys. Fluids*, **33**, 095120.
- Yan, X., Liang, X., Ouyang, W., Liu, Z., Liu, B., Lan, J. 2017, A review of progress and applications of ship shaft-less rim-driven thrusters, *Ocean Eng.*, **144**, 142–156.
- Zhang, Y., Vanierschot, M. 2021, Proper orthogonal decomposition analysis of coherent motions in a turbulent annular jet, *Appl. Math. Mech.-Engl.*, **42**, 1297–1310.
- Zhu, W., Gao, H. 2019, A numerical investigation of a winglet-propeller using an LES model, *J. Mar. Sc. Eng.*, **7**, 333.